On-Chip Digital Fourier-Transform Spectrometer Using a Thermo-Optical Michelson Grating Interferometer

Richard A. Soref, *Life Fellow, IEEE, Fellow, OSA*, Francesco De Leonardis, Vittorio M. N. Passaro, *Senior Member, IEEE, Senior Member, OSA*, and Yeshaiahu Fainman, *Fellow, IEEE, Fellow, OSA*

***Abstract*—This theoretical modeling and simulation paper presents designs and projected performance of an on-chip digital Fourier transform spectrometer using a thermo-optical (TO) Michelson grating interferometer operating at ∼1550 and 2000 nm for silicon-on-insulator and for germanium-on-silicon technological platforms, respectively. The Michelson interferometer arms consist of two unbalanced tunable optical delay lines operating in the reflection mode. They are comprised of a cascade connection of waveguide Bragg grating resonators (WBGRs) separated by a piece of straight waveguide with lengths designed according to the spectrometer resolution requirements. The length of each WBGR is chosen according to the Butterworth filter technique to provide one resonant spectral profile with a bandwidth twice that of the spectrometer bandwidth. A selectable optical path difference (OPD) between the arms is obtained by shifting the notch in the reflectivity spectrum along the wavelength axis by means of a low-power TO heater stripe atop the WBGR, inducing an OPD that depends on the line position of the WBGR affected by TO switching. We examined the device performances in terms of signal recostruction in the radio-frequency (RF) spectrum analysis application at 1 GHz and at 1.5 GHz of spectrometer resolution. The investigation demonstrated that high-quality spectrum reconstruction is obtained for both Lorentzian and arbitrary input signals with a bandwidth up to 40 GHz. We also show that spectrum reconstruction of 100–200 GHz RF band input signals is feasible in the Ge-on-Si chips.**

***Index Terms*—Bragg grating resonators, microwave photonics, spectrometer, true time delays.**

Manuscript received June 11, 2018; revised July 24, 2018; accepted August 13, 2018. Date of publication August 27, 2018; date of current version October 25, 2018. The work of R. A. Soref was supported by the Air Force Office of Scientific Research under Grant FA9550-17-1-0354. The work of Y. Fainman was supported by the National Science Foundation. The work of V.M.N. Passaro was supported by Fondo di Ricerca di Ateneo 2012. *(Corresponding author: Vittorio M. N. Passaro.)*

R. A. Soref is with the Department of Engineering, The University of Massachusetts Boston, Boston, MA 02125 USA (e-mail: soref@rcn.com).

F. De Leonardis and V. M. N. Passaro are with the Photonics Research Group, Department of Electrical and Information Engineering, Politecnico di Bari, Bari 70125, Italy (e-mail: francesco.deleonardis@poliba.it; vittorio.passaro@poliba.it).

Y. Fainman is with the Department of Electrical and Computer Engineering, University of California, San Diego, La Jolla, CA 92093-0407 USA (e-mail: yfainman@ucsd.edu).

Color versions of one or more of the figures in this paper are available online at http://ieeexplore.ieee.org.

Digital Object Identifier 10.1109/JLT.2018.2867241

I. Introduction

THIS theoretical paper proposes and analyzes a new ultra-high-resolution Michaelson interferometer that functions as an on-chip 64-channel digital Fourier-transform spectrometer (dFTS). The main application investigated here is radio-frequency (RF) spectrum analysis by an integrated optical-microwave system-on-a-chip. For this chip, the light source is a laser "carrier" that is amplitude-modulated by an incoming RF spectrum whose profile is not known. The carrier and both RF sidebands occupy an optical frequency range of about 50 GHz, for example, which calls for at least ∼1 GHz resolution to determine the RF profile in detail.

An examination of the literature on prior- art on-chip FTS's, shows several recent papers [1]–[3] that describe a digitally addressed Mach-Zehnder interferometer (dFTS) in which the spectrometer resolution is 0.49 nm within the optical band centered at 1550 nm. Here we propose an alternative architecture based on this digital approach for high-resolution applications. There is an analogy here to the traditional bulk-optics FTS where an electro-mechanical Michelson interferometer (MI) is employed. Here the MI is a monolithic semiconductor waveguide device that is scanned without moving parts using the thermo-optical (TO) effect. The novelty in the present work consists in several aspects: i) the single MI operates in the reflective mode, giving the needed interferograms via unbalanced MI arms; ii) a selectable optical path difference (OPD) between the arms which is generated using two groups of identical waveguide Bragg-grating resonators (WBGRs) having a peak in transmission and a notch in reflection; iii) only one resonator in each arm is tuned by low-power TO to choose the optical path of each arm; iv) the arm-addressing scheme starts with all gratings in transmission and changes only one to reflection by shifting its profile along the wavelength axis; v) each resonator is a composite of several closely coupled phase-shifted gratings; vi) a single photodetector on-chip is used to record the interferograms; vii) a compact multi-spiral waveguide approach is proposed to provide a compact footprint for the dFTS, despite the few-cm length of one MI arm; viii) the dFTS architecture applies to Ge-on-Si (GOS) chips for the mid infrared, as well as to SOI; ix) the dFT applies to other high-resolution uses and x) most importantly, a spectrometer frequency-resolution

of 1.0 to 1.5 GHz is predicted here for a custom design. In fairness to the prior approaches [1]–[3]. we note that they share the aforementioned features of compact spirals, one photodiode, GOS, and high resolution. However, our approach offers a factor-of-two reduction in the maximum arm length required.

The paper is organized as follows. In the background discussion of Section II, the prior art is discussed in the context of the present dFTS. Section III presents the chip layout and our MI addressing technique. Signal reconstruction analysis is performed in Section IV, where several parametric simulations are performed for spectrometers based on both SOI and GOS platforms, operating at 1 GHz and at 1.5 GHz of resolution. Moreover, detailed analysis is presented in order to demonstrate the spectrum reconstruction of RF signals ranging from 15 to 100 GHz of bandwidth. The GOS chip is able to provide larger spectrometer bandwidth than the SOI chip due to germanium's ~3x larger TO coefficient. Finally, the conclusions are summarized in Section V.

II. Background Discussion

In the literature on prior-art on-chip FTSs, the principal approach taken has been to utilize a large number of progressively unbalanced Mach-Zehnder interferometers (MZIs) on a chip, such as 32 MZIs that are co-integrated on the same chip with 32 photodetectors, each PD dedicated to its MZI, resulting in a fairly complex chip [4]–[6]. Some alternatives to this multiple-MZI approach were reported recently [7]–[10]. The first method is to utilize only one MZI in which the two connecting arms are identical and quite long, ~ 34 mm for example [10]. There, a TO microheater is placed atop one of the two spiraled arms that then can provide a continuously variable, analog OPD between arms by modifying the waveguide effective index of only one arm (thermal expansion can come into play, too). The issue there is the rather limited repertoire of OPDs available (the small values produced) since the TO effect induces only one or two parts-per-thousand changes in index. The second approach takes a two-bus-coupled micro-ring resonator, a ring TO tuned, as the spectral input to a single balanced MZI having TO shifting of one of its arms. It is a fine approach but the limited OPD there gave somewhat limited FTS resolutions in the 0.14 to 0.47 nm range. An unusual and modern approach is the digital FTS invented in [1]–[3]. It is indeed a broadband spectrometer where a clever addressing method was adopted. A set of unequally joined 2×2 MZI cross-bar switches selects the effective length of each arm simultaneously in a compact arrangement where three switching stages offered 64 different OPDs. That work explored moderately high resolution but did not examine the specialized microwave-photonic RF application in which extremely high resolution is required. The present proposed 64-channel dFTS technique substitutes MI for MZI, uses reflection rather than transmission, avoids the use of any cross-bar switches, and relies instead upon TO shifting of a narrowband reflective grating, employing a temperature rise of 50 K or less in mid-grating. The large OPDs that are feasible in the MI by coiling up its arms are beneficial for realizing extremely high resolution; but at the same time there is a penalty to be paid in the spectrometer bandwidth (*BW*). This observation bandwidth shrinks down to a very small value since $BW = N_{ch} \times \delta\lambda$ where N_{ch} is the channels number and $\delta\lambda$ is the resolution. This BW reduction is, however, acceptable for the microwave applications. We should point out an intrinsic disadvantage of the proposed architecture, which is the quadratic scaling law between N_{ch} the number of spectral channels and N_s the number of switches: $N_{ch} = (N_s/2)^2$. Indeed, for the 64 channel-dFTS, our device requires 16 WBGRs compared to 6 switches obtained in [2] where the scaling is exponential $N_{ch} = 2^{Ns}$. Our quadratic scaling law can represent a bottleneck for applications in which a very large number of channels is required. Also, if we go outside of the radio frequency applications where lower resolution is accepted in order to cover a broad observation BW, then the grating BW will enter as a constraint that will limit the observation range and will prevent octave-spanning observations, for example.

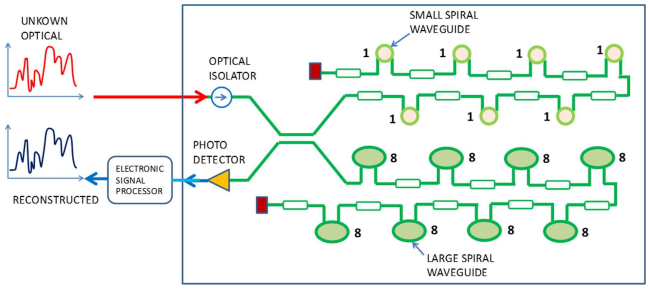

Fig. 1. On-chip layout of a digital Fourier transform spectrometer using a thermo-optical Michelson grating interferometer.Each red square represents an optical absorber. In the picture the numbers "8" and "1" indicate that the spiral lengths are in the ratio 8:1.

III. On-Chip Spectrometer Architecture

The on-chip 64-channels spectrometer architecture is sketched in Fig. 1. The unknown-profile input signal is sent to the two arms of the Michelson interferometer by means of a 3 dB directional coupler. Each arm consists of 8 cascaded WBGRs separated by spiral waveguides of length $0.5 \times \Delta L$ and $4 \times \Delta L$ for the shorter and longer arm, respectively, where the value of ΔL is determined on the basis of the spectrometer resolution requirements and represents the separation between the center of two adjacent WBGR. Moreover, a $4 \times \Delta L$ long spiral waveguide at the input of the longer arm is required in order to generate 64 different OPDs in the range from ΔL to $64 \times \Delta L$. The WBGR elements are notch-reflection gratings that are implemented by inserting a phase-shifting segment within the grating. It is assumed here that this spectral profile can be easily shifted along the wavelength axis by means of a low-power heater stripe atop the grating, in the same manner that we previously described for WBGRs deployed in the arms of Mach-Zehnder interferometer devices [11]–[13] for the functions of tunable optical filtering and switching. The spectrometer operation can be explained with the aid of Fig. 2, where the TO-programming is shown in detail. The wavelength of operation (purple dashed line) is λ_0. At the rest condition, all TOs are switched OFF and all identical WBGR transmissions are aligned at the same wavelength λ_0, as in Figs. 2(a) and 2(b). Under this condition the overall structure has no reflection and

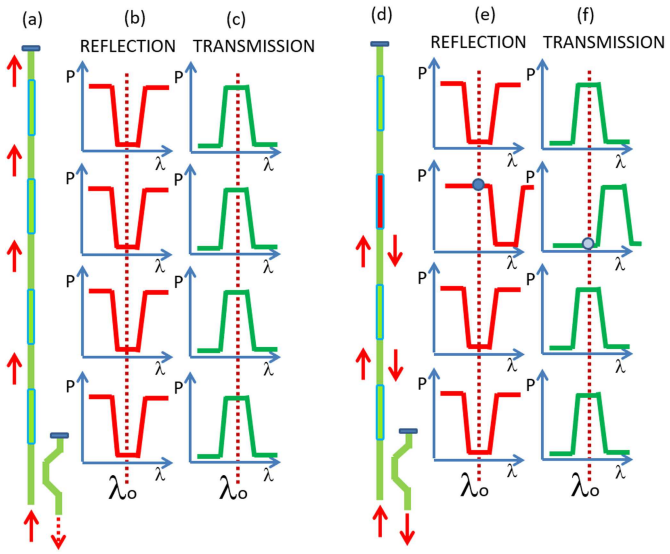

Fig. 2. Type-1 addressing of a TO-programmble waveguide optical "delay line arm" using notch-R WBGRs for the selection of any one of four optical lengths. Here λ_0 is the wavelength of operation: (a) initial unheated line; (b) unheated R profiles; (c) unheated T profiles; (d) TO selection of third-grating; (e) shift of R profile; (f) shift of T profile.

no signal is detected at the output of the directional coupler. When a particular WBGR is tuned to a different wavelength by turning its heater ON (a wavelength adequately separated from λ_0 to induce low cross-talk, i.e., CT, Fig. 2(d)), then the light arriving at that spatial location is reflected, as presented in Figs. 2(e) and 2(f). This shift of spectral profile induces a particular round trip path that depends upon the line position of the WBGR affected by TO switching (see Ref. [14] for details). As a result of switching different TO pairs in the MI arms, 64 different OPDs can be selected in progressing steps of ΔL.

In this context according to [3] the spectrometer resolution can be estimated as:

$$\delta\lambda = \frac{\lambda_0^2}{n_g N_{ch} \Delta L} \tag{1}$$

where n_g is the group effective index; taken as 4.2395 for SOI and 4.6238 for GOS.

Turning again to the architecture of Fig. 1, the 3 dB directional coupler performs the interference between the signal reflected from both MI arms. Thus, the interferogram for each TO combination is recorded at the detector output. In this sense, the intensity measured by the detector for an arbitrary input signal (represented by a column vector $\boldsymbol{x}$ with n elements) is [3]:

$$\mathbf{y} = \mathbf{A}\mathbf{x} \tag{2}$$

where the interferogram $\boldsymbol{y}$ is a column vector with 64 elements, each gives the detector output at a particular TO combination. The ensemble of spectra forms a $64 \times n$ calibration matrix $\mathbf{A}$. Each row of $\mathbf{A}$ represents a reflectance spectrum and contains n elements, the number of wavelength points in the scan. Each column corresponds to a discretely sampled interferogram and contains 64 elements. It is worth outlining that since $\boldsymbol{x}$ is an unknown signal, the interferogram vector $\boldsymbol{y}$ recorded to the detector output can be interpreted as the predictor to be used together with the matrix $\mathbf{A}$ to reconstruct the input signal spectrum by minimizing the associated L_1 and L_2 norms via elastic net regression methods [15], [16].

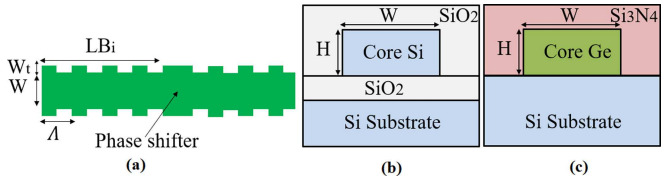

Fig. 3. (a) Top view of SOI strip waveguide showing the geometry of one phase-shifted Bragg-grating resonator that is used in a set of closely coupled resonators; (b) SOI waveguide cross section; (c) GOS waveguide cross section.

IV. Numerical Results

The goal of this section is to present the design for the on-chip spectrometer using thermo-optical Michelson grating interferometer. In particular, we propose parametric simulations to evaluate the reconstruction quality, assuming different types of input signals. Then, the performance of the spectrometer system operating at 1550 nm in the SOI platform and at 2000 nm in the GOS platform is evaluated.

A. 64-96 GHz Spectrometer Bandwidth

The individual resonant structure used in the MI architecture is a cascade of N closely end-coupled waveguided Bragg grating resonators as described in detail in [11]–[13]. One constituent resonator of the overall WBGR is illustrated in Fig. 3(a), where the fundamental design parameters are indicated. Such N-combining allows for engineering of the spectral profile (such as side walls and bandwidth BW_g) of the N-coupled structure.The N-WBGR is realized in a single-mode wire waveguide as sketched in Fig. 3(b) and 3(c) for the SOI and GOS platforms, respectively. The unperturbed cross section is $W \times H = 450 \times 250$ nm, and $W \times H = 700 \times 500$ nm, for the single TE-mode SOI and GOS waveguides, respectively.

The Bragg grating sections are created by introducing along the nanowire, sidewall corrugations having width extension $W_t = 100$ nm. The period is chosen to be $\Lambda = 315$ nm and 273.65 nm in order to operate at the central wavelength λ_0 of 1550 nm and 2000 nm in the case of SOI and GOS, respectively. The separation between individual resonators is zero in our work. Hereafter, the length of the first Bragg resonator is given as $LB_1 = M \times \Lambda$, where M is the number of periods in the Bragg section of the first WBG. In addition, the lengths LB_i $(i = 2 \ldots N)$ have been designed as a function of LB_1 in order to induce the Butterworth transmittivity response. Moreover, all simulations are performed using a mixed full-vectorial mathematical model based on the FEM, CMT and Transfer Matrix approaches (see Ref. [11] for details). Several parametric simulations indicate that the signal reconstruction improves greatly if the condition $BW_g \sim 2\,BW_s$. We take this result as an important design rule for the dFTS. In this context, we consider two different WBGR structures, having $N = 3$, $M = 20$, $LB_1 = 6.3\,\mu$m, $BW_g = 130$ GHz and $N = 3$, $M = 57$, $LB_1 = 15.6\,\mu$m, $BW_g = 125.44$ GHz, for the SOI and GOS platforms, respectively.

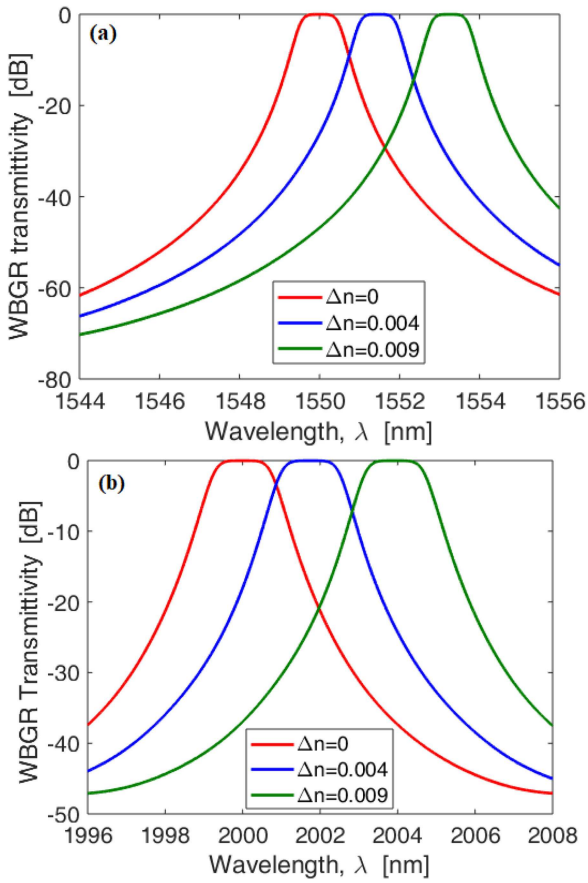

Fig. 4. WBGR transmittivity spectrum for different values of Δn; (a) SOI: $W = 450$ nm, $H = 250$ nm, $N = 3$, $M = 20$, $W_t = 100$ nm, and $\alpha_1 = 0.5$ dB/cm. (b) GOS: $W = 700$ nm, $H = 500$ nm, $N = 3$, $M = 57$, $W_t = 100$ nm, and $\alpha_1 = 0.5$ dB/cm.

Having determined two representative notch-R gratings, Figs. 4(a) and 4(b) show the WBGR transmittivity spectra for different values of the TO-induced refractive index change (Δn) and for SOI and GOS, respectively.

The plot of Fig. 4 indicates that by setting $\Delta n(SOI) = 0.004$ and $\Delta n(GOS) = 0.009$, a wavelength shift of 1.453 nm from $\lambda_0 = 1550$ nm *(SOI)* with a CT $= -27$ dB and a *(GOS)* shift of 3.913 nm from $\lambda_0 = 2000$ nm with CT $= -37.72$ dB can be recorded. Moreover, due to the silicon and germanium thermo-optic coefficient $dn/dT = 1.86 \times 10^{-4}$ K^{-1}, and 5.8×10^{-4} K^{-1} a local temperature change of $\Delta T \sim$ 21.5, and 15.51 K are expected for the spectrometers based on SOI or GOS platform, respectively. Note that a shift of 12.6 nm is feasible in GOS for $\Delta T = 50$ K.

Next, we examine the operation of our dFT spectrometer based on the thermo optical Michelson grating interferometer at both 1 GHz and 1.5 GHz of resolution (δf). In Table I we summarize the geometrical parameters of the MI spectrometer.

Table I shows that the GOS provides a ~30% reduction in the MI arms lengths. Let us now examine specifics about the total spectrometer size (footprint) and the spirals required. We consider the worst-case scenario that is represented by the SOI platform operating at 1 GHz of resolution where the 35.38 mm MI long-arm length must be accommodated. There, each spiral has a waveguide length of 4.26 mm including its two short connectors. We thus will examine 4-mm-length spirals in the long arm. For their construction, we shall take our cues from the experiments of [10] where each arm of their MZI consisted of a rectangular spiral having a footprint of about 0.25 mm $\times$1 mm for a 30.4 mm waveguide length, using 5 μm waveguide spacing, and right-angle waveguide bends with a bend radius of 10 μm. For our dFTS, this spiral compression factor implies an area of 0.033 mm^2 for our 4 mm spirals, which could for example, be a rect-spiral of 200 μm $\times$ 166 μm footprint. For that reason, it is likely that the entire Fig. 1 dFTS could fit on a silicon chip of the order of 8 mm $\times$ 4 mm for example.

The reflectivity spectra of the device for all 64 perturbations of the on/off TO combinations are plotted in Figs. 5(a) and

TABLE I
GEOMETRICAL PARAMETERS OF THE MI SPECTROMETER

	Spectrometer resolution: δλ=1 GHz		Spectrometer resolution: δλ=1.5 GHz	
	SOI	GOS	SOI	GOS
WBGR length: [μm]	40.77	57.87	40.77	57.87
ΔL [mm]	1.11	1.01	0.74	0.67
Short arm length [mm]	3.91	3.60	2.62	2.42
Long arm length [mm]	35.38	32.44	23.59	21.63

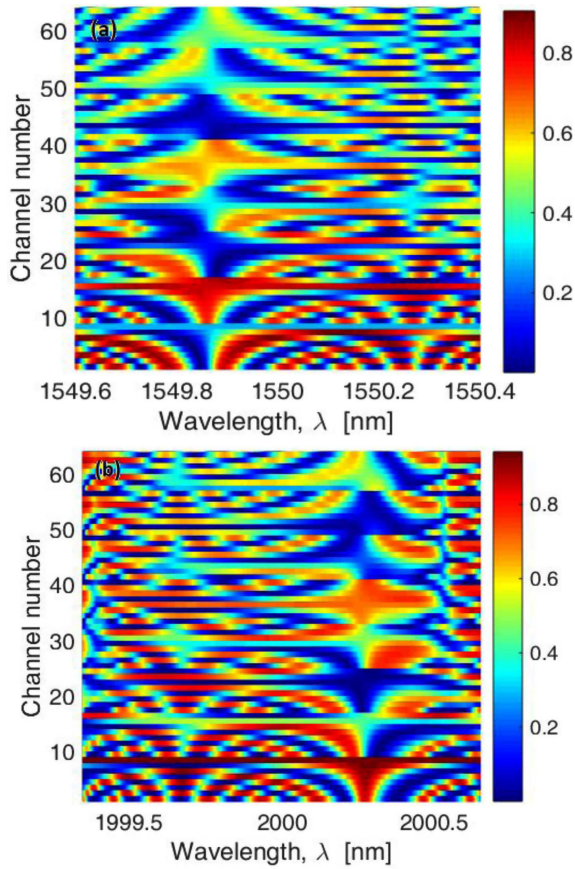

Fig. 5. Reflectivity as a function of the number channel and the optical wavelength: (a) SOI: $W = 450$ nm, $H = 250$ nm, $N = 3$, $M = 20$, $W_t = 100$ nm, and $\alpha_1 = 0.5$ dB/cm; (b) GOS: $W = 700$ nm, $H = 500$ nm, $N = 3$, $M = 57$, $W_t = 100$ nm, and $\alpha_1 = 0.5$ dB/cm. The simulations are performed at 1 GHz of resolution.

5(b), for SOI and GOS respectively, where the spectrometer resolution is 1 GHz.

In the simulations, we have assumed the corrugation width (W_t), and the propagation loss coefficient (α_l) of 100 nm and 0.5 dB/cm, respectively. The WBGR shift spectrum is created by the TO-induced refractive index change of $\Delta n = 0.004$ and 0.009 for SOI and GOS techological platform, respectively. Moreover, the TE polarization, specifically the TE_{00}–like fundamental optical mode, has been assumed in our analysis. In order to isolate thermally the passive spirals in Fig. 1 from the TO-perturbed gratings, an air trench can be etched underneath the short connecting waveguides going to the spirals. Thereby the spirals gain some thermal isolation from suspended connectors, as desired. Also, some air trenches can be etched in the over-cladding dielectric to add thermal isolation.

The ensemble of 64 reflectivity spectra shown in Fig. 5 represents the basis set for spectrum reconstruction based on elastic net regularized regression method.

To demonstrate the principle of behaviour of the MI spectrometer, we apply the reconstruction technique to two types of input signals: Lorentzian profiles with different linewidth, and generic polychromatic signals.

For the specific MI spectrometer based on the SOI platform, Figs. 6(a)–6(d) show the recostructed spectra for $\delta f =$ 1 GHz and 1.5 GHz, assuming in input Lorentzian signals having the FWHM (δf_{FWHM}) ranging from 15 to 70 GHz. Our simulations indicate that the device is able to reconstruct the input signal in its fundamental features such as shape and bandwidth. Moreover, the reconstruction quality is very high up to a FWHM value around 40 GHz. Unwanted ripples appear when the input signal presents a bandwidth approaching the spectrometer bandwidth $(BW_s = 64$ or 96 GHz$)$. To test the reconstruction quality, we apply at the input of the SOI spectrometer an arbitrary input spectra having several dips and peaks. The results are plotted in Figs. 7(a)–7(c), confirming that a very high quality recostruction can be obtained for arbitrary input signal up to 40 GHz of bandwidth. Similar systematic investigations have been performed for the spectrometer using a thermo-optical Michelson grating interferometer realized in the GOS platform.

The numerical results are condensed in Fig. 8, and lead to the same conclusions made for the SOI platform, although showing some discrepancies for the GOS realization at 1.5 GHz of resolution. It is worth outlining that the simulations of Fig. 8 have been performed for given geometrical parameters optimized at 1 GHz of resolution. Thus, the condition $BW_g \sim 2\,BW_s$ at 1.5 GHz of resolution is not satisfied, inducing some discrepancies in the signal recostruction.

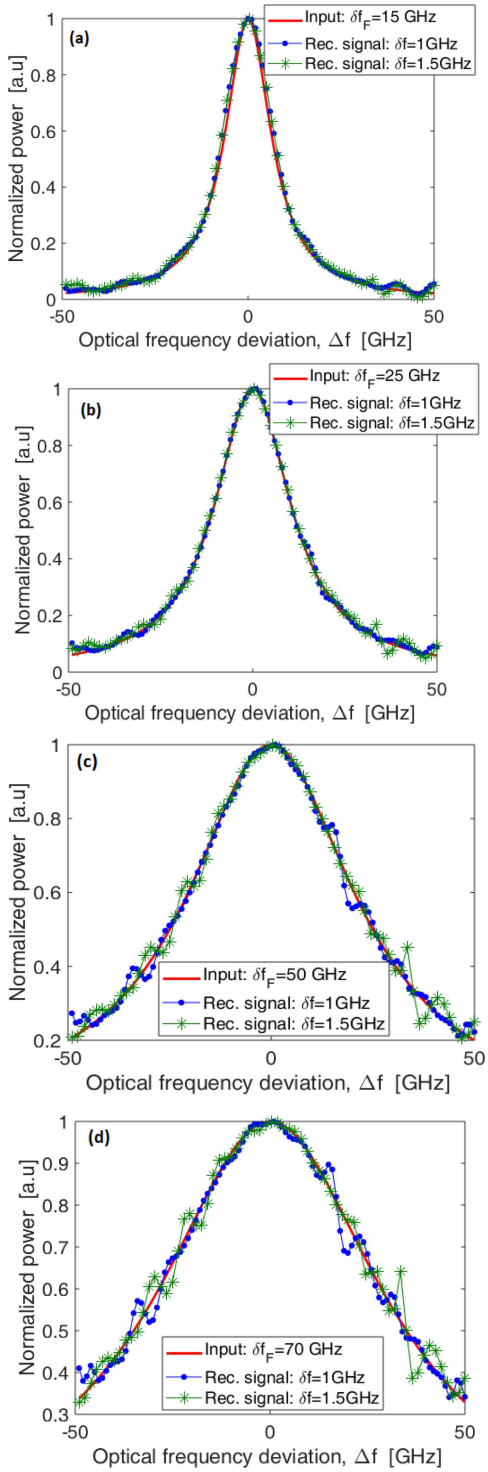

Fig. 6. Signal recnostruction for different input Lorentzian signals (red solid lines) (a) FWHM = 15 GHz; (b) FWHM = 25 GHz; (c) FWHM = 50 GHz; (d) FWHM = 70 GHz. The simulations are performed by considering:c64 channels, 1 GHz (dot) and 1.5 GHz (asterisk) of resolution in SOI platform.

B. 243 GHz Spectrometer Bandwidth

In this sub-section we investigate the feasibility of reconstructing an RF signal with large bandwidth of 100 GHz. In this context we assume the architecture of Fig. 1 having a resolution $\delta f = 3.8$ GHz corresponding to a $BW_s = 243.2$ GHz. Thus, an RF BW up to ∼200 GHz could actually be accepted. The relationship $BW_g \sim 2\,BW_s$ implies that only the GOS platform is to be used for the 100-200 GHz RF BW dFTS. This happens because large values of BW_g require large TO tuning in order to adequately separate the center WBGR wavelength from λ_0. Due to the ∼3x larger thermo-optic coefficient, germanium can guarantee a large value of Δn but with a moderate local heating. Therefore in the following analysis, we consider the WBGR

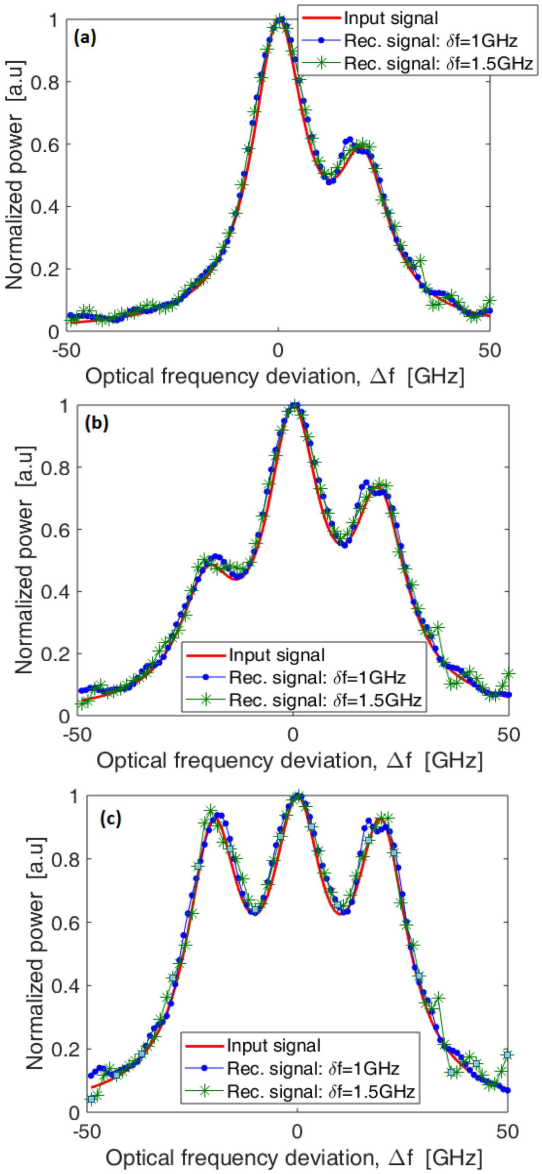

Fig. 7. (a)–(c) Signal reconstruction for arbitrary input signals (red solid lines). The simulations are performed by considering: 64 channels, 1 GHz (dot) and 1.5 GHz (asterisk) of resolution in SOI platform.

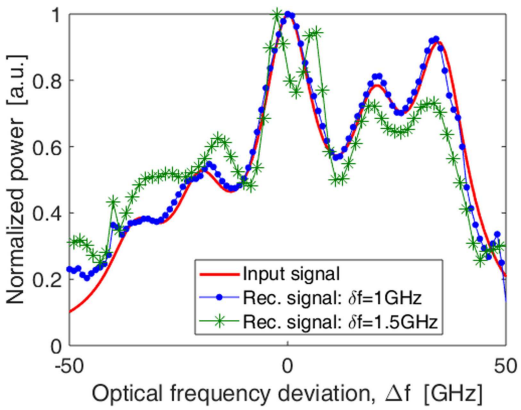

Fig. 8. Signal reconstruction for arbitrary input signals (red solid lines). The simulations are performed by considering: 64 channels, 1 GHz (dot) and 1.5 GHz (asterisk) of resolution in GOS platform.

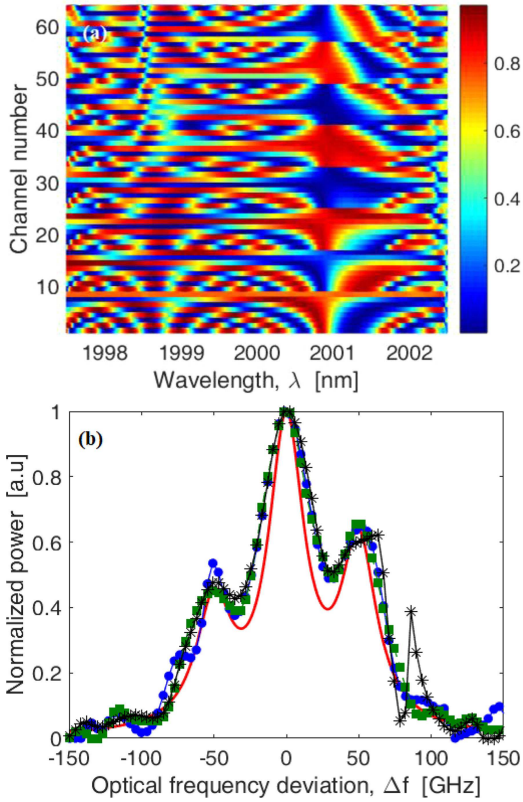

Fig. 9. (a) Reflectivity as a function of the number channel and the optical wavelength; (b) Signal reconstruction for arbitrary input signals (red solid lines); dot: $\delta f = 3.8$ GHz, $\mathrm{E}_{\Delta \mathrm{L}} = 0\%$; square: $\delta f = 3.8$ GHz, $\mathrm{E}_{\Delta \mathrm{L}} = 10\%$; asterisk: $\delta f = 3.8$ GHz, $\mathrm{E}_{\Delta \mathrm{L}} = 15\%$; The simulations are performed by considering: 64 channels, in GOS platform: $W = 700$ nm, $H = 500$ nm, $N = 3$, $M = 30$, $W_t = 100$ nm, and $\alpha_1 = 0.5$ dB/cm.

structures, having $N = 3$, $M = 30$, $LB_1 = 8.2$ μm, and then $BW_g = 500.6$ GHz. The value $\Delta n(GOS) = 0.018$ has been assumed to induce a wavelength shift of about 7.884 nm (589 GHz) with CT $= -17$ dB. Moreover a local temperature change of ΔT$\sim$ 31 K is expected.

Looking at the architecture of Fig. 1, we estimate $\Delta L = 0.267$ mm, yielding GOS MI arm lengths of 8.53 mm and 0.99 mm, respectively.

In this context, taking a "wide" arbitrary RF band, Fig. 9(a) shows the reflectivity spectra of the GOS dFTS for all 64 perturbations of the on/off TO combinations, assuming the spectrometer resolution is 3.8 GHz. On the basis of the interferograms plotted in Fig. 9(a), the retrieved signal is shown in Fig. 9(b) indicating that an arbitrary input signal with a bandwidth around 100 GHz can be reconstructed with a good quality. Moreover, Fig. 9(b) shows the realistic scenario in which phase errors take place as induced by an error ($\mathrm{E}_{\Delta \mathrm{L}}$) in the designed value ΔL. In the worst-case scenario, we have assumed that all the spiral waveguides are affected by the aforementioned errors. The simulations reveal that the main part of the spectrum is accurately retrieved up to $\mathrm{E}_{\Delta \mathrm{L}} = 10\%$, with a weak broadening around the secondary peak at $\Delta f = -50$ GHz. However, this plot also demonstrates degradation of the retrieved spectrum for $\mathrm{E}_{\Delta \mathrm{L}} > 15\%$ as result of the presence of unwanted virtual artefacts (spikes).

The dFTS chip is in an environment with an ambient temperature, and realistically there will be small fluctuations in that ambient. This then raises the question of how the spiral's "performance" will be modified by minor changes in the spiral waveguide's effective index induced by chip temperature changes. We have examined this question, and proceeding in a manner similar to that taken in Fig. 9(b), we speculate that thermally induced optical-phase errors of up to 10% on each waveguide spiral can be accepted with no strong effects upon the retrieved spectrum. For the case of larger phase errors, this requires the technique of calibration (see Ref. [18]) in order to eliminate degradation of the retrieved spectrum. As mentioned above, thermal isolation techniques are available. Generally, we estimate that added thermal controllers are not required for the spirals.

The GOS dFTS is expected to operate well over the 2 to 16 μm wavelength range because the GOS-MI waveguided circuit is quite transparent over that range, and because the TO coefficient stays about the same over that range. For operation at any central wavelength λ_0 greater than 2 μm and less than 6 μm, the strip waveguide $W \times H$ dimensions and the grating tooth extensions W_t would all be scaled up appropriately from their 2 μm values. Taking ΔT$\sim$ 50 K as an upper limit, which gives $\Delta n = 0.029$, we then calculated the wavelength-shift of the grating profile $\Delta\lambda_{\rm sh}$ at values of λ_0 at the low end and at the high end of the range. We found that the shifted profile experienced -17 dB of optical crosstalk when we took BW_g as 72% of $\Delta\lambda_{\rm sh}$. Using that BW_g and taking $BW_g \sim 2\,BW_s$, we then determined that $BW_s = 0.22\%$ of λ_0 for any λ_0 in the GOS transparency range. Considering both SOI and GOS platforms, we see that all resonant structures in the MI arms have nanometer-scale features that require high precision in the fabrication. In practice, there will always be fabrication errors related to dimensional inaccuracies in the WBGR grating. If dimensional errors $\Delta\Lambda$ are made in fabricating the period, deviation from λ_0 by an amount, $\Delta\lambda_{\rm tol}$, occurs. In this context quantitative estimations are proposed in our recent works [11], [12]. Generally speaking, the way to minimize fabrication errors is to manufacture the chip in an advanced, high resolution, CMOS foundry. Even so, a few WBGR errors would remain, however, their effect can be minimized. The approaches available to do this were discussed in [17]. The techniques include employing micron-scale direct-current TO heaters on the arms to "trim" their response on a constant basis, and/or to deposit atomic-layer films on the arms to offer permanent trimming of any imbalances.

V. Conclusions

In this paper, a novel, manufacturable on-chip thermo-optical Michelson grating interferometer for Fourier spectral reconstruction application is proposed and analyzed theoretically. The digitally addressed chip consists of two different-length tunable delay lines, operating in reflection mode. Each delay line is based on notch-reflection gratings that are implemented by inserting a phase-shifting segment within the grating in order to realize a resonatnt peak in transmission. Waveguide Bragg grating resonators consisting of *N* closely coupled resonators are used here as active devices. The *N* value and the cavity grating lengths have been chosen to satisfy the Butterworth filter technique, resulting here in a filter profile with high peak transmission, and a bandwidth twice that of the spectrometer bandwidth according to our optimization procedure. The 2x design rule is related to bandwidth narrowing effects in each delay line. Grating sections are constructed by extending numerous uniform "teeth" laterally beyond the width of the TE single-mode strip waveguide. The unperturbed waveguide cross sections of 450 $\times$ 250 nm and 700 $\times$ 500 nm have been considered for silicon on insulator and germanium on silicon technological platforms, respectively. The device generates 64 selectable optical path differences between the MI arms, by tuning only one particular resonator in each arm using low-power TO. A single photodetector on-chip is used to record these 64 interferograms. On the basis of these interferograms, the RF spectrum reconstruction has been investigated for both Lorentzian and arbitrary input signals. The simulations have demonstrated that high quality reconstructions are feasible for RF-modulated input bandwidth up to 40 GHz, by assuming spectrometer resolutions of 1 GHz or 1.5 GHz. In this context, the larger WBGR spacing in the longer MI arm has been estimated as 7.04 mm and 4.68 mm for SOI (1.55 μm) and GOS (2 μm), respectively. Thus, spiral waveguide-connecting structures have been assumed between adjacent WBGRs. Moreover, spectrum recostruction of an input RF signal with 100 GHz of bandwidth (well within the $\rm BW_s$ of 243 GHz) has been obtained in the GOS platform assuming a spectrometer resolution of 3.8 GHz, and a local temperture change of about 31 K. Regarding chip losses, we find that as the optical spectrum travels from chip input to photodiode, it experiences a loss comprised of 6 dB directional coupler loss (3 dB worse than in [2]), plus a variable loss due to traversal of the delay lines. In the worst case, the variable loss is 14 IL_g where IL_g is the transmission loss of one WBGR. An overall maximum loss of about 10.2 dB is estimated for the case where $IL_g = 0.3$ dB. Moreover, in the worst-case scenario (for the 64$^{\rm th}$ channel), we record an extinction-ratio reduction from 24.7 dB to 16.52 dB for the propagation losses ranging from 0.25 dB/cm to 3 dB/cm. Beneficially, in this range, simulations indicate that the impact upon the spectrum reconstruction is negligible. In addition, if we consider the results of differential attenuation between the two arms of the MI [19], we do find unwanted oscillatory features with unphysical negative values that take place in the peripheral spectral regions. However, despite those effects, the main part of the spectral reconstruction is still preserved.

References

[1] D. M. Kita *et al.*, "On-chip infrared spectroscopic sensing: Redefining the benefits of scaling," *IEEE J. Sel. Topics Quantum Electron.*, vol. 23, no. 2, Mar./Apr. 2017, Art. no. 5900110.

[2] D. M. Kita *et al.*, "Digital Fourier transform spectroscopy: A high-performance, scalable technology for on-chip spectrum analysis," 2018. [Online]. Available: https://arxiv.org/pdf/1802.05270.

[3] D. M. Kita *et al.*, "High-resolution on-chip digital Fourier transform spectroscopy," in *Proc. Conf. Lasers Electro-Opt.*, 2018, Paper SF1A.1.

[4] A. V. Velasco *et al.*, "High-resolution Fourier-transform spectrometer chip with microphotonic silicon spiral waveguides," *Opt. Lett.*, vol. 38, pp. 706–708, 2013.

[5] M. Piels and D. Zibar, "Compact silicon multimode waveguide spectrometer with enhanced bandwidth," *Sci. Rep.*, vol. 7, 2017, Art. no. 43454.
[6] M. Nedeljkovic, A. V. Velasco, A. Z. Khokhar, A. Delâge, P. Cheben, and G. Z. Mashanovich, "Mid-infrared silicon-on-insulator Fourier-transform spectrometer chip," *IEEE Photon. Technol. Lett.*, vol. 28, no. 4, pp. 528–531, Feb. 2016.
[7] B. Redding, S. F. Liew, Y. Bromberg, R. Sarma, and H. Cao, "Evanescently coupled multimode spiral spectrometer," *Optica*, vol. 3, pp. 956–962, 2016.
[8] S. N. Zheng, L. K. Chin, and A. Q. Liu, "On-chip spectrometer enhanced by ring resonator cavity: High-resolution and large-bandwidth," in *Proc. Conf. Lasers Electro-Opt.*, 2017, Paper JTh2A.119.
[9] S. N. Zheng, Y. Y. Chen, H. Cai, Y. D. Gu, and A. Q. Liu1, "High-resolution and large-bandwidth on-chip microring resonator cavity-enhanced Fourier-transform spectrometer," in *Proc. Conf. Lasers Electro-Opt.*, 2018, Paper ATh4O.2.
[10] M. Souza, A. Grieco, N. C. Frateschi, and Y. Fainman, "Fourier transform spectrometer on silicon with thermo-optic non-linearity and dispersion Correction," *Nature Commun.*, vol. 9, pp. 1–8, 2018. doi: 10.1038/s41467-018-03004-6.
[11] R. Soref, F. De Leonardis, and V. M. N. Passaro, "Mach-Zehnder cross-bar switching and tunable filtering using N-coupled waveguide Bragg resonators," *Opt. Express*, vol. 26, no. 12, pp. 14959–14971, 2018.
[12] R. Soref, F. De Leonardis, and V. M. N. Passaro, "Reconfigurable optical-microwave filter banks using thermo-optically tuned Bragg Mach-Zehnder devices," *Opt. Express*, vol. 26, no. 12, pp. 14879–14893, 2018.
[13] R. Soref, F. De Leonardis, and V. M. N. Passaro, "Tunable optical-microwave filter optimized for 100 MHz resolution," *Opt. Express*, vol. 26, no. 14, pp. 18399–18411, 2018.
[14] R. Soref, F. De Leonardis, and V. M. N. Passaro, "Integrated on-chip Bragg time-delay system for thermo-optical control of a microwave antenna," *J. Lightw. Technol.*, submitted for publication.
[15] H. Zou and T. Hastie, "Regularization and variable selection via the elastic net," *J. Roy. Statist. Soc., Series B (Statist. Methodol.)*, vol. 67, pp. 301–320, 2005.
[16] S. Shalev-Shwartz and S. Ben-David, *Understanding Machine Learning: From Theory to Algorithms*. Cambridge, U.K.: Cambridge Univ. Press, 2014.
[17] J. R. Hendrickson, R. Soref, and R. Gibson, "Improved 2 × 2 Mach–Zehnder switching using coupled-resonator photonic-crystal nanobeams," *Opt. Lett.*, vol. 43, no. 2, pp. 287–290, 2018.
[18] A. Herrero-Bermello *et al.*, "Temperature dependence mitigation in stationary Fourier-transform on-chip spectrometers," *Opt. Lett.*, vol. 42, no. 11, pp. 2239–2242, 2017.
[19] K. Okamoto, H. Aoyagi, and K. Takada, "Fabrication of Fourier-transform, integrated-optic spatial heterodyne spectrometer on silica-based planar waveguide," *Opt. Lett.*, vol. 35, no. 12, pp. 2103–2105, 2010.

Richard A. Soref (LF'03) received the Ph.D. degree in electrical engineering from Stanford University, Stanford, CA, USA, in 1964, after which he embarked upon a 54-year career in basic and applied research in the fields of nonlinear optics, materials science, liquid-crystal displays, free-carrier modulators, waveguide theory, opto-electronics, microwave photonics, sensors, photonic-integrated circuits, laser physics, plasmonic-photonics, photonic crystals, and infrared detection. He is known as the "father of silicon photonics" for his visionary, fundamental contributions to the science and technology of silicon photonics. He is currently a Research Professor of engineering with the University of Massachusetts at Boston. He has authored or coauthored more than 540 papers, has written 11 book chapters, and holds 54 U.S. patents. His works are listed on Google Scholar with 20,386 citations, a Hirsch index of 68, and an i-10 index of 251. He is a Fellow of the National Academy of Inventors, The Optical Society, Air Force Research Laboratory, and the Institute of Physics U.K.

Francesco De Leonardis received the Laurea and Ph.D. degrees in electronic engineering from the Politecnico di Bari, Bari, Italy, in 1999 and 2003, respectively. Since 2004, he has been a Research Assistant with the Politecnico di Bari, and a member with the Photonics Research Group. He has authored or coauthored more than 150 papers in international journals and conference presentations and holds one international patent. His research interests include mainly the fields of integrated optical sensors and nonlinear photonic devices.

Vittorio M. N. Passaro (S'92–SM'05) received the Laurea (*cum laude*) and Ph.D. degrees in electronic engineering from the Politecnico di Bari, Bari, Italy, in 1988 and 1992, respectively. Since October 2000, he has been with the Politecnico di Bari as an Associate Professor of electronics. Since 2004, he has been the Founder and the Leader of the Photonics Research Group, Politecnico di Bari. He has authored or coauthored more than 350 papers in optoelectronics and photonics topics, published in international journals (one by *Nature Photonics*) and conference proceedings. He holds two international patents and is the Editor of five scientific books (one by Springer). He is a senior member of the Optical Society of America and an associate member of the National Institute of Nuclear Physics.

Yeshaiahu Fainman received the M.Sc. and Ph.D. degrees from Technion, Haifa, Israel, in 1979 and 1983, respectively. He is an inaugural Cymer Chair Professor of Advanced Optical Technologies and a Distinguished Professor of Electrical and Computer Engineering with the University of California, San Diego (UCSD). He is directing research of the Ultrafast and Nanoscale Optics group, UCSD, and made significant contributions to near-field optical phenomena, inhomogeneous and metamaterials, nanophotonics and plasmonics, and nonconventional imaging. His current research interests include near-field optical science and technology with applications to information technologies and biomedical sensing. He has authored or coauthored more than 300 manuscripts in peer review journals and more than 500 conference presentations and conference proceedings. He is a Fellow of the Optical Society of America, Fellow of the Society of Photo-Optical Instrumentation Engineers, and a recipient of the Miriam and Aharon Gutvirt Prize, Lady Davis Fellowship, Brown Award, Gabor Award, Emmett N. Leith Medal, and Joseph Fraunhofer Award/Robert M. Burley Prize.